Frictional experiments of dolerite at intermediate slip rates with controlled temperature: Rate weakening or temperature weakening?

Hiroyuki Noda,[1,2] Kyuichi Kanagawa,[3] Takehiro Hirose,[4] and Atsuyuki Inoue[3]

Received 24 August 2010; revised 8 April 2011; accepted 29 April 2011; published 26 July 2011.

[1] A rotary shear apparatus has been newly set up in Chiba University which can control the temperature near a sliding surface, T_{meas}, up to 1000°C independently from slip rate, V. Frictional experiments at 0.010 m/s, 1 MPa normal stress, and variable T_{meas} for dolerite have revealed a remarkable effect of temperature on the friction coefficient, f. With increasing T_{meas}, f starts from 0.7 to 0.8 at room temperature (RT), decreases down to 0.5–0.6 at 400°C, increases until 800°C, and then decreases again. We have also conducted XRD analyses of the wear materials (mainly submicron particles) and investigated microstructures of the sliding surfaces developed at different temperatures T_{meas}, and we found that there is a negative correlation between f and the amount of amorphous material except at RT and 1000°C. The generation of the amorphous phase probably causes the weakening. There is no amorphous phase recognized for a sample at 1000°C which is an aggregate of rounded crystals. EBSD analyses show that the material on the sliding surface at 1000°C contains randomly oriented hematite grains, which together with the observed microstructural features suggests that granular flow was taking place. We have also demonstrated that f depends not only on the instantaneous value of temperature, but also on its history. By comparing with conventional rotary shear friction experiment for the same dolerite without temperature control, we conclude that strong "rate weakening" as recently observed in high-velocity frictional experiments without an active control of the temperature has a significant amount of contribution from the temperature effect.

Citation: Noda, H., K. Kanagawa, T. Hirose, and A. Inoue (2011), Frictional experiments of dolerite at intermediate slip rates with controlled temperature: Rate weakening or temperature weakening?, *J. Geophys. Res.*, *116*, B07306, doi:10.1029/2010JB007945.

1. Introduction

[2] A strong "rate-weakening" frictional behavior has been observed experimentally at seismic slip rates for many types of rocks at different conditions in terms of the history of the slip rate, V, the normal stress, σ_n, and the chemical environment [e.g., *Prakash and Clifton*, 1992; *Tsutsumi and Shimamoto*, 1997a; *Beeler et al.*, 2008]. This behavior is frequently explained by a variety of thermal weakening mechanisms depending on the rock type and the experimental condition, including an intrinsic temperature weakening of microscopic contacts and an increase in macroscopic temperature T on a fault which is defined for a much larger representative elementary volume than microscopic asperities [*Noda*, 2008], flash heating of microscopic contacts or local temperature rise at the true contacts even without a large increase in T [*Rice*, 1999, 2006; *Beeler et al.*, 2008; *Noda*, 2008], melt lubrication [e.g., *Hirose and Shimamoto*, 2005], phase transformation and generation of weak materials [e.g., *Goldsby and Tullis*, 2002; *Han et al.*, 2007] and so on. These thermal weakening mechanisms proposed so far are sensitive to T. Note that T is different from the average of the local temperature at the true contacts. The latter could be substantially higher than the former because of a small fraction of the true contact area to the nominal fault area. High slip rates and thus high heat generation rates cause an increase in T in the experiments as well as in the natural coseismic slip events, but its evolution is probably substantially different. This is because of the difference in the history of V, in σ_n, and in the thermal properties of the surrounding medium. In order to properly interpret existing experiments and to formulate a frictional constitutive law applicable to earthquake simulations, it is important to understand the effects of T and V separately.

[3] In the previous frictional experiments at high slip rates, T is increased by frictional heating and there is no active

[1]Seismological Laboratory, California Institute of Technology, Pasadena, California, USA.
[2]Now at Institute for Research on Earth Evolution, Japan Agency for Marine-Earth Sciences and Technology, Yokohama, Japan.
[3]Department of Earth Sciences, Chiba University, Chiba, Japan.
[4]Kochi Institute for Core Sample Research, Japan Agency for Marine-Earth Science and Technology, Nangoku, Japan.

0148-0227/11/2010JB007945

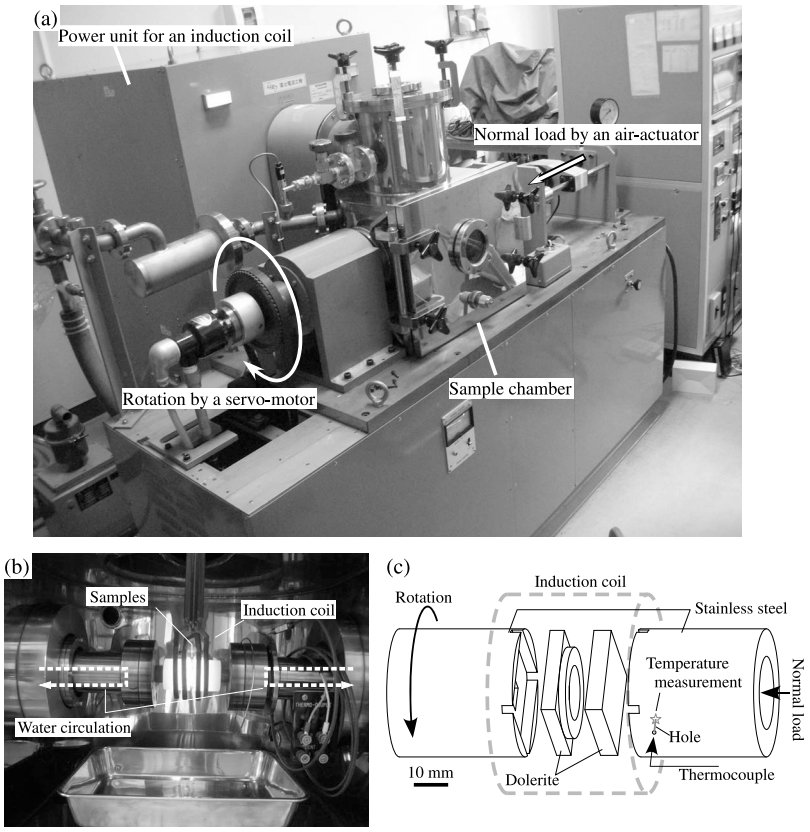

Figure 1. A rotary shear deformation apparatus for friction at high slip rates and temperatures (HTVR). (a) A photograph of the apparatus. (b) A photograph of the sample assembly. The central bright potion is heated up to 1000°C. (c) A schematic diagram of the sample assembly.

control of it. In such experiments, the steady state value and evolution of T and thus the friction coefficient, f, measured as a function of the slip rate, V, depends on the thermal properties of the apparatus; the steady state temperature distribution depends on the thermal properties and the shape of the apparatus and a boundary condition around it. For example, if the heat capacity near the simulated fault is larger, then the evolution of T becomes milder for the same frictional heat production rate. Although there are earlier efforts to monitor T during experiments [*Tsutsumi and Shimamoto*, 1997b; *Han et al.*, 2007], it is essentially important to control T and V independently to investigate their effects separately.

[4] The effects of T on f has been investigated at low slip rates typically below 1 mm/s [e.g., *Shimamoto*, 1986; *Chester*, 1994; *Blanpied et al.*, 1995]. The effect of dynamically evolving T becomes more important at higher slip rates because of the significant frictional heating.

[5] In recent numerical studies on dynamic rupture propagation, [e.g., *Noda et al.*, 2009; *Noda and Lapusta*, 2010] coseismic and interseismic changes in temperature have been calculated, including a feed back to the frictional resistance mainly through pore pressure buildup (thermal pressurization [*Rice*, 2006, and references therein]). The improvement in the frictional constitutive law accounting for the temperature is a key to more mechanically and geologically realistic numerical simulations. Note that there are many geological studies on the detection of coseismic frictional heating and temperature rise to give constraints on the mechanical behavior of a fault [*O'Hara*, 2004; *Murakami and Tagami*, 2004; *Fukuchi et al.*, 2005; *Kano et al.*, 2006; *Tanaka et al.*, 2006; *Hamada et al.*, 2009].

[6] Thus friction experiments at controlled T and V independently are needed in order not only to separate their effects on the frictional strength, but also to incorporate them into the friction constitutive law. For such experiments, we have newly installed a rotary shear deformation apparatus for frictional sliding with a temperature control [*Senda et al.*, 1992, 1995] (HTVR) at Chiba University. This paper presents the effect of temperature on the friction coefficient of dolerite at a wide range of temperatures from room temperature (RT) to 1000°C. In addition, we have conducted a series of friction experiments at intermediate to high slip rates with a high-velocity friction apparatus at Kochi Core Center (HVR), the same apparatus used by *Tsutsumi and Shimamoto* [1997a, 1997b], measuring the temperature of the frictional

Table 1. List of Experiments Conducted With HTVR

Run Number	Type of Experiment	T_{meas} (°C)
HTVR010	Constant T_{meas}	800
HTVR011	Constant T_{meas}	RT
HTVR012	Constant T_{meas}	600
HTVR013	Constant T_{meas}	200
HTVR014	Constant T_{meas}	400
HTVR015	Constant T_{meas}	1000
HTVR016	Increasing T_{meas} by steps	RT to 1000 every 100
HTVR017	T_{meas} cycle	RT, 50, 500, 50, 500, 50

Table 2. List of Experiments Conducted With HVR

Run Number	V (m/s)
HVR1873	0.010, 0.023, 0.049, 0.101, 0.206, 0.414
HVR1874	0.010
HTR1875	0.010
HVR1876	0.049
HVR1877	0.206
HVR1878	0.101
HVR1879	0.101

surface using a pyrometer. By comparing those two series of experiments, we discuss the effects of T and V on the frictional strength separately.

2. Experimental Methodology

2.1. Frictional Apparatuses

[7] Frictional experiments have been conducted using a high velocity and high temperature rotary shear apparatus at Chiba University (Figure 1a) (HTVR). This apparatus was originally developed by *Senda et al.* [1992, 1995] in collaboration with Fuji Electronic Industrial Co., Ltd. to study the friction of ceramics. The normal load is applied by an air actuator, and the torque by a servo-controlled motor. The sample assembly is inside a chamber in which we can control the atmospheric environment by evacuating air or filling up of chemically nonreactive gas. Because the torque is measured outside the sample chamber, one of the O rings around the shaft in stationary side likely accounts for a part of the torque. This effect is discussed later in comparison with the experimental data using a high velocity friction apparatus at Kochi Core Center (HVR) [*Tsutsumi and Shimamoto*, 1997a, 1997b]. Currently the maximum rotation rate, normal load, torque are 500 rpm, 490 N, and 4.8 Nm, respectively.

[8] A photograph and a schematic diagram of the sample assembly of HTVR are shown in Figures 1b and 1c, respectively. A pair of rock samples as described below is placed on a set of sample holders made of stainless steel. A high-frequency induction coil surrounding the sample holders is used to heat up the sample holders and also the rock samples. Cooling water is circulated inside shafts so that temperature is high only near the samples. We can control a measured temperature, T_{meas}, by tuning the power input to the induction coil with an accuracy of 1°C using a proportional–integral–derivative controller. The temperature on the surface of a sample holder can be increased by about 5°C/sec at most. The maximum cooling rate which is achieved by turning off the induction coil depends on the temperature since the cooling is done mainly by the circulating water. In the runs at room temperature (RT) in which the induction coil is turned off, T_{meas} increases due to frictional heating which cannot be avoided. *Senda* [2004] reported a heating experiment of alumina at a heating rate of 120°C/min up to 1000°C, and showed that the temperature on the surface of a sample holder becomes stable within 1°C in about 2 min after it reaches to 1000°C.

[9] The samples for HTVR are two square-shaped plates (25 mm × 25 mm × 5 mm and 25 mm × 25 mm × 4 mm) and the thinner of them has a flat doughnut (2 mm thick) on it (Figure 1c). The outer and inner diameters of the simulated fault are 25 mm and 15 mm, respectively. Using samples of this size, the maximum area-averaged slip rate and normal stress are 0.5 m/s and 1.56 MPa, respectively. The square shape prohibits the samples from rotating freely from the holders. In the experiments presented in this paper, a thermocouple is put in a hole on the side of one of the sample holders to measure and control temperature, T_{meas}, at 7 mm away from the fault (2 mm from the rock/stainless interface) and 11 mm from the axis of rotation. In the experiments reported in this study, T_{meas} is only modestly different from the temperature on the sliding surface T as discussed in the following section.

[10] We have also conducted supplemental friction experiments using a high velocity friction apparatus at Kochi Core Center (HVR) [*Tsutsumi and Shimamoto*, 1997a, 1997b] at various slip rates V. In these runs, the temperature on the fault T changes due to frictional heating and thermal conduction away from the sliding surface. Although there is no active control on T in this series of experiments, we measured it at the periphery of the sliding surface using a pyrometer which can measure temperatures up to 500°C with a focal spot size of 1.2 mm. We have used hollow cylindrical specimens with 15 mm and 25 mm inner and outer diameters so that the shape and the size of the sliding surfaces are the same as those for HTVR runs.

2.2. Sample Description

[11] We have used a dolerite from Belfast, Northern Ireland as rock samples. This dolerite is composed mainly of plagioclase (44.5%) and clinopyroxene (27.9%) with minor amounts of hornblende (9.3%), quartz (5.8%), K-feldspar (3.6%), orthopyroxene (3.6%), biotite (1.8%), apatite (0.8%), and opaque minerals (2.7%) including magnetite, hematite and ilmenite. It shows an ophitic texture of euhedral lath-shaped plagioclase and anhedral clinopyroxene. Grain size ranges from 50 μm to 1 mm. The samples were shaped by a surface grinder machine so that the variation in the thickness within a sample is less than 10 μm.

2.3. Experimental Procedure

2.3.1. Experiments With HTVR

[12] The experiments using HTVR have been conducted at a normal stress, σ_n = 1 MPa and a slip rate, V = 0.010 m/s. We have conducted two types of experiments, some at a fixed T_{meas}, and the others at several T_{meas} changed by steps while the sliding is held. After the former type of experiments, we have collected the wear materials in addition to the samples, and their microstructures have been investigated. In experiments of the latter type, we can avoid the difference due to similar but different samples, and examine the effect of temperature history as well as that of instantaneous value of T. All experimental conditions for HTVR runs are listed in Table 1.

[13] After a pair of samples was set on the holders, they were slid relative to each other for 100 m as presliding at the experimental condition. Then the simulated fault was slid for about 10 m in each run. Note that in experiments with steps in T_{meas} while the sliding is held, we do not open the sliding surface and no presliding is conducted between 2 experiments at different T_{meas}. At RT, T_{meas} increases by about 7°C and remains steady during presliding. This is the temperature rise due to frictional heating. If we consider

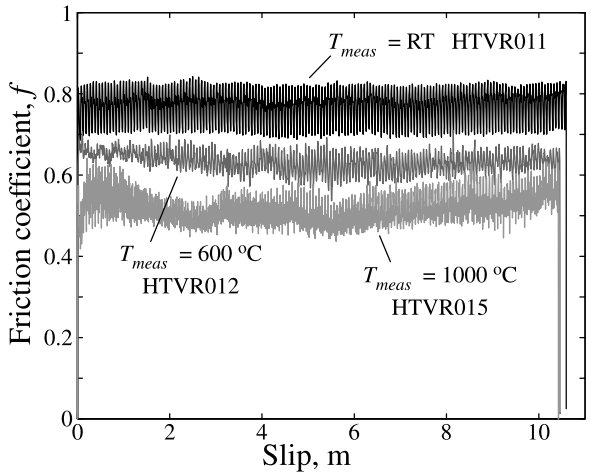

Figure 2. Characteristic mechanical behavior during HTVR runs at $\sigma_n = 1$ MPa and $V = 0.010$ m/s. Oscillations are every 1 revolution of samples. No remarkable slip weakening is observed.

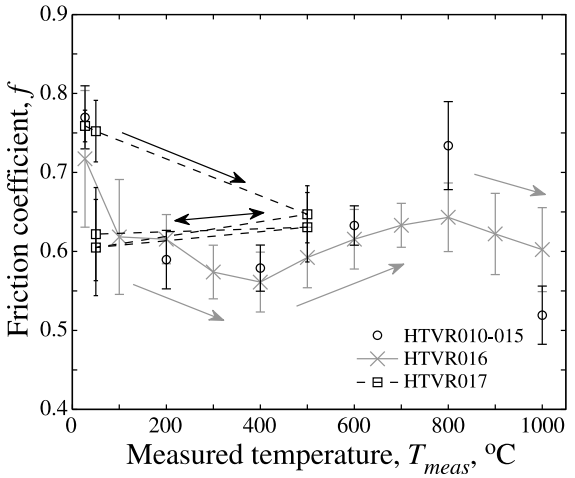

Figure 3. Summary of HTVR runs. Data points are connected by lines when a same sample is used, with arrows indicating the order of experiments.

1 dimensional steady state temperature distribution with fixed temperature at the point where the cooling water reaches under an assumption that the total heat flow along the rotation axis is proportional to temperature gradient, heat conductivity (2 W/mK for the rock sample and 16 W/mK for stainless steel), and the cross-sectional area, then the temperature on the simulated fault plane T, is higher than T_{meas} by about 6°C. This is much smaller than the differences in T_{meas} in different experiments. Therefore, the effect of frictional heating has only a minor temperature effect in comparing data obtained in this study.

2.3.2. Experiments With HVR

[14] The experiments using HVR have been conducted at $\sigma_n = 1$ MPa and $V = 0.010$–0.414 m/s which are low enough to avoid the generation of frictional melt. We have used the same normal stress as the HTVR runs in order to avoid a complexity in comparing the two sets of experiments. We follow the same procedure reported in previous studies using the same apparatus [e.g., *Tsutsumi and Shimamoto*, 1997a, 1997b]; after specimens are set in the apparatus, we preslid the samples until the frictional surfaces become parallel. In one of the experiments, HVR 1873, the slip rate V is changed by steps from 0.010 m/s to 0.414 m/s. HVR 1874 to 1879 are runs with constant V. All experimental conditions for HVR runs are listed in Table 2.

3. Experimental and Observational Results

3.1. Mechanical Properties

3.1.1. Experiments With HTVR

[15] Figure 2 shows raw data for some characteristic experiments, HTVR011 (RT), 012 (600°C), and 015 (1000°C). Uniform shear stress for a simulated fault is assumed to calculate the friction coefficient f. It varies within the range of around ±0.1 during every sample rotation, but the differences between experiments at different T_{meas} can be clearly distinguished. No remarkable weakening with increasing slip displacement (slip weakening) is recognized in the HTVR runs, although there are minor long-range fluctuations.

[16] Figure 3 summarizes the HTVR runs. Note that T_{meas} is the measured temperature which is controlled, and the actual temperature on the fault, T, is probably higher by 4 to 6°C if we can simply add the contribution due to frictional heating estimated in the last section. The data points and

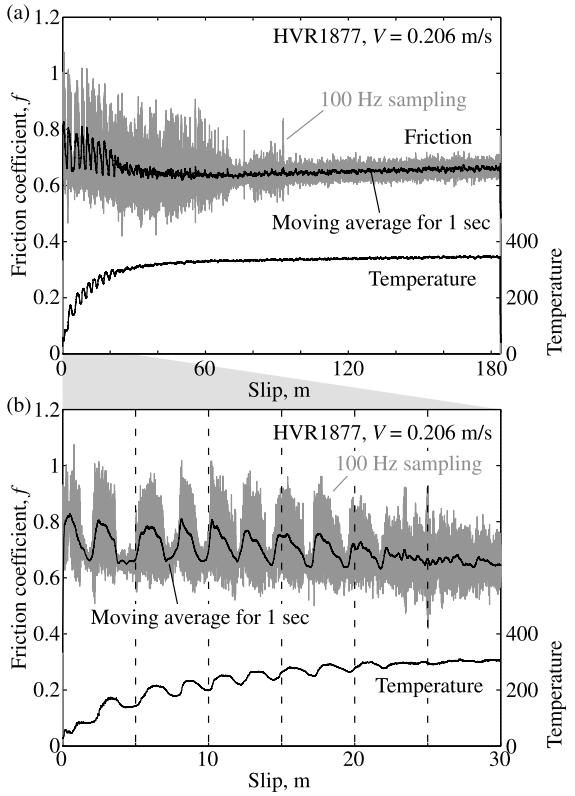

Figure 4. A characteristic mechanical behavior and the temperature measured by a pyrometer of HVR runs. (a) Before the temperature on the fault is stabilized, weakening takes place on average. (b) Magnified image during transient change in the temperature, showing a positive correlation between the friction coefficient and temperature.

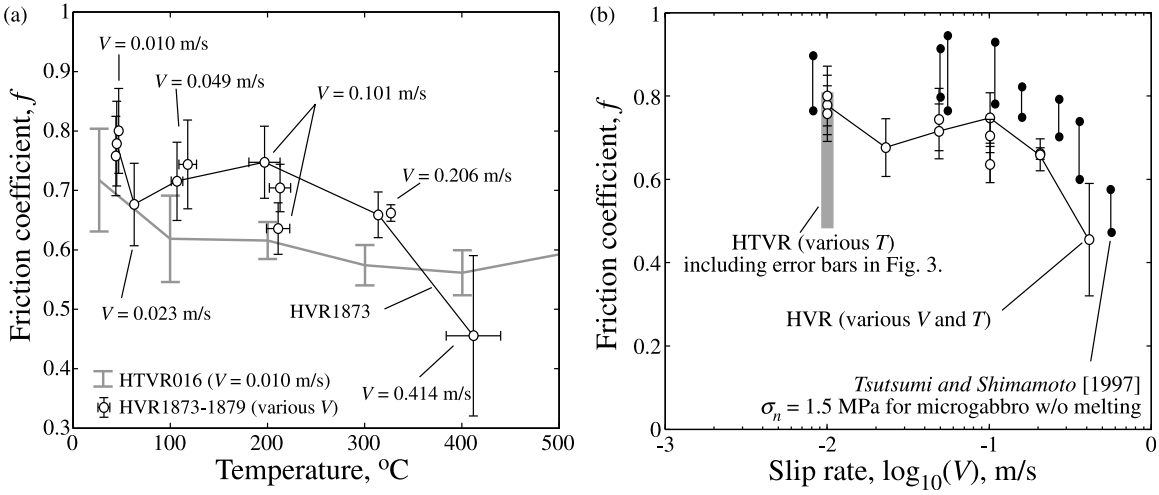

Figure 5. Friction coefficient for HVR runs in which the temperature on the fault is not actively controlled. The data points are connected with lines when a same sample is used. (a) Friction coefficient, f, as a function of the temperature measured. HTVR016 in which V is kept constant at 0.010 m/s is plotted as well. The error bars represent one standard deviation of the raw data which are plotted if longer than the white circle. (b) Friction coefficient, f, as a function of V. The range of data from HTVR runs are indicated by a gray bar at V = 0.01 m/s. Mechanical data by *Tsutsumi and Shimamoto* [1997a, 1997b] is plotted as well for reference.

the error bars respectively represent averages and standard deviations of f from 8 m to 10 m in slip. Data points are connected by lines if the same sample is used.

[17] At RT, f is 0.7–0.8 which agrees with Byerlee's law [*Byerlee*, 1978]. With increasing T, f decreases down to 0.5–0.6 at 400°C, then increases until T reaches 800°C, and finally decreases again. This behavior is observed for experiments at fixed T_{meas} for different samples (black circles in Figure 3) as well as for a series of experiments with monotonically increasing T_{meas} for an identical set of samples (HTVR016, gray crosses in Figure 3).

[18] Experiments with cycles in T_{meas} between 50°C and 500°C (HTVR017, black squares in Figure 3) show that f depends not only on the instantaneous value of temperature, but also on its history. In the first and second experiments at T_{meas} = RT and 50°C, f is about 0.75, and decreases to about 0.65 in the third one at T_{meas} = 500°C. When we decrease T_{meas} to 50°C, f stays at the same level as that at 500°C or even decreases slightly though error bars are long, instead of recovering to the initial values.

3.1.2. Experiments With HVR

[19] Figure 4 represents typical mechanical behavior of HVR runs (HVR1877 at 0.206 m/s, as an example). In this particular run, frictional heating is efficient enough to cause significant temperature rise at the frictional surface as measured by the pyrometer. Although the friction coefficient f

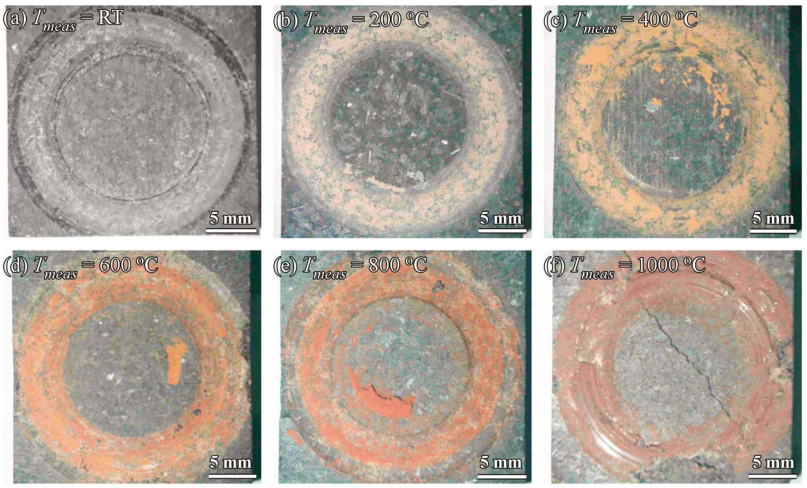

Figure 6. Photographs of sliding surfaces after experiments. (a) HTVR011 (RT), (b) HTVR013 (200°C), (c) HTVR014 (400°C), (d) HTVR012 (600°C), (e) HTVR010 (800°C), and (f) HTVR015 (1000°C). Scale bars are 5 mm in length.

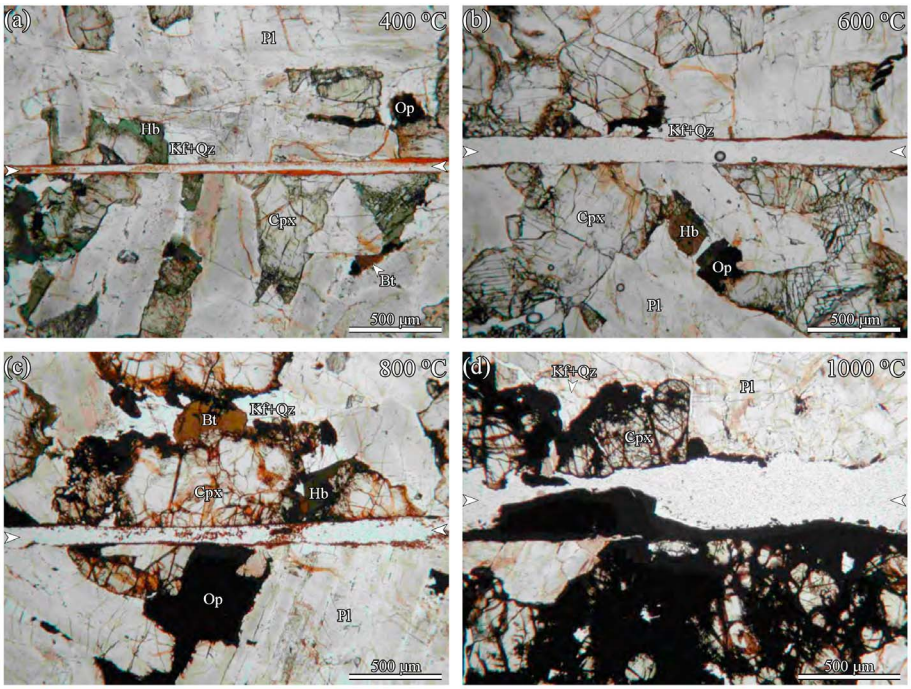

Figure 7. Optical micrographs under plane-polarized light of the sections across the sliding surfaces. (a) HTVR014 (400°C), (b) HTVR012 (600°C), (c) HTVR010 (800°C), and (d) HTVR015 (1000°C). Scale bars are 500 μm in length. Pl, plagioclase; Cpx, clinopyroxene; Hb, hornblende; Bt, biotite; Kf, K-feldspar; Qz, quartz; Op, opaque minerals.

scatters, f decreases on average as the temperature increases (slip < 40 m in Figure 4a). If this initial part is magnified, however, there is a positive correlation between f and temperature (Figure 4b). An increase in f and thus in heat generation rate contributes to the temperature rise. In order to fully understand the observed transient behavior, it is important to formulate f as a function of temperature and state variables [e.g., *Chester*, 1994], and to consider the mechanical and thermal interaction between the simulated fault and its surrounding medium.

[20] Nearly steady state values of f and temperature are measured from the time histories like Figure 4a; in the particular case of HVR1877, we take the average and standard deviation of f and the temperature in the final 10 m of slip. Figures 5a and 5b shows the experimental data after projected onto (T, f) and (V, f) planes, respectively, together with some of the data points from HTVR for reference. The horizontal axis in Figure 5a represents T_{meas}, the temperature measured at 7 mm from the fault for HTVR runs, and temperature measured by the pyrometer of the fault surface for HVR runs. Note that for HTVR runs, the temperature rise due to frictional heating is small because of a low slip rate (see section 2.3.1). Overall, f decreases with increasing T if T < 400°C and with increasing V. Only from the HVR data, it is difficult to conclude whether the weakening is due to the effect of T or that of V. The comparison of HTVR and HVR is discussed later.

3.2. Macroscopic and Microscopic Observations of the Samples

[21] Figure 6 shows the sliding surfaces after HTVR runs at fixed T_{meas} from RT to 1000°C. Wear materials are observed on the sliding surfaces after the experiments at temperatures from RT to 800°C, the color of which changes gradually from gray at RT through orange at 400°C to reddish brown at 800°C (Figures 6a–6e). In contrast, a chocolate paste-like solid material with grooves is observed on the sliding surface after the experiment at 1000°C (Figure 6f).

[22] Optical microscope observations reveal that hornblende remains greenish in color until T_{meas} of 400°C (e.g., Figure 7a), while it becomes brownish above T_{meas} of 600°C (e.g., Figures 7b and 7c). At T_{meas} of 1000°C, hornblende is not found. Accordingly, the amount of opaque minerals increases with increasing T_{meas} (Figure 7).

[23] Electron microscope observations reveal that materials on the sliding surfaces below T_{meas} of 800°C are essentially wear particles (e.g., Figure 8a). Although they contain comminuted angular crystalline particles larger than 1 μm in diameter, they are largely composed of extremely fine-grained powder particles smaller than 100 nm or even 10 nm in diameter (e.g., Figure 8b). In contrast, the material on the sliding surface at T_{meas} of 1000°C exhibits a flowage and folded structure (Figure 8c). It consists of very fine-grained (largely smaller than 1 μm in diameter), rounded and equant particles of plagioclase, clinopyroxene, quartz, magnetite and hematite (Figure 8d), and shows a rather homogeneous mixture. In the host rock at T_{meas} of 1000°C, clinopyroxene grains have symplectite rims composed of fine-grained (100 nm to 3 μm in diameter) vermicular clinopyroxene, plagioclase, magnetite and hematite (Figures 8e and 8f).

3.3. X-Ray Diffraction Analyses

[24] We have done X-ray diffraction analyses on the wear materials at T_{meas} from RT to 800°C as well as on the material

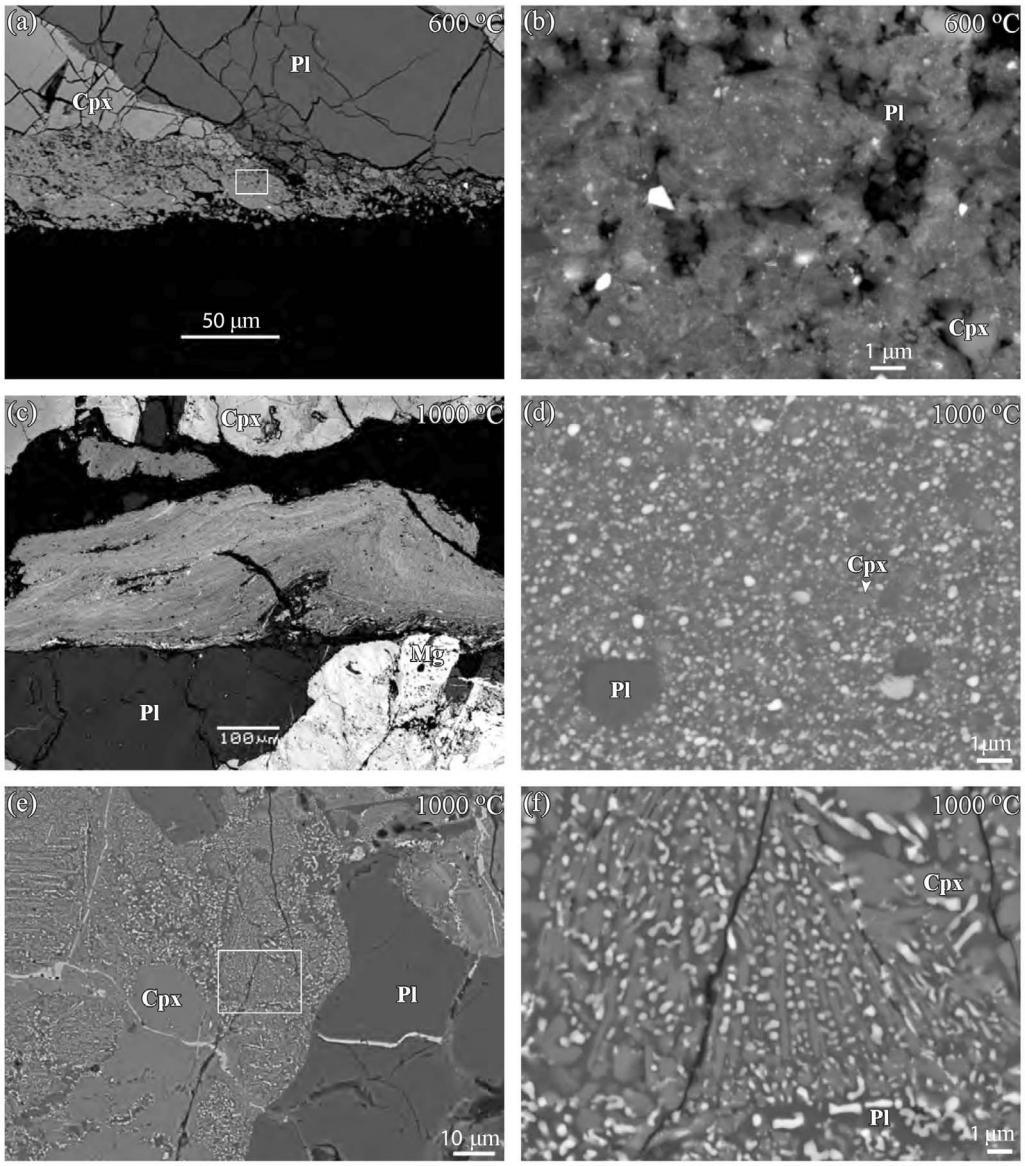

Figure 8. Backscattered electron micrographs of samples. (a) Section across the sliding surface of HTVR012 (600°C). (b) Enlarged view of the rectangle area shown in Figure 8a. (c) Section across the sliding surface of HTVR015 (1000°C). (d) Enlarged view of an area of the material on the sliding surface in Figure 8c. Light gray and white grains are magnetite and hematite. (e) Symplectite rim of a clinopyroxene grain in the host rock of HTVR015 (1000°C). (f) Enlarged view of the rectangle area shown in Figure 8e. Light gray and white grains are magnetite and hematite. Pl, plagioclase; Cpx, clinopyroxene; and Mg, magnetite.

on the sliding surface at T_{meas} of 1000°C. Clasts of the host dolerite were removed by sieving, and only wear materials smaller than 250 μm in size were used for X-ray diffraction analyses. Because clasts of the material on the sliding surface at T_{meas} of 1000°C were also found together with wear materials collected, they were hand picked and prepared for X-ray diffraction analyses. We used a sample holder made of nonreflective glass in order to appropriately identify and quantify amorphous phase.

[25] Qualitative analyses of the wear materials reveal a broad peak above the background in addition to sharp peaks of plagioclase, quartz, clinopyroxene, magnetite and hematite (e.g., Figure 9a), suggesting the presence of amorphous phase as revealed for wear materials from rotary shear experiments by *Yund et al.* [1990]. It may be argued that such a broad peak as observed is possibly due to the presence of extremely fine-grained crystalline particles smaller than a few nm in size. If the wear materials consist totally of crystalline particles, the observed X-ray diffraction profiles of sharp peaks and a broad peak as shown in Figure 9a would require a bimodal grain size distribution of crystals larger than a few μm for example and those smaller than a few nm. However, such bimodal grain size distribution is unlikely, because comminution is known to produce a

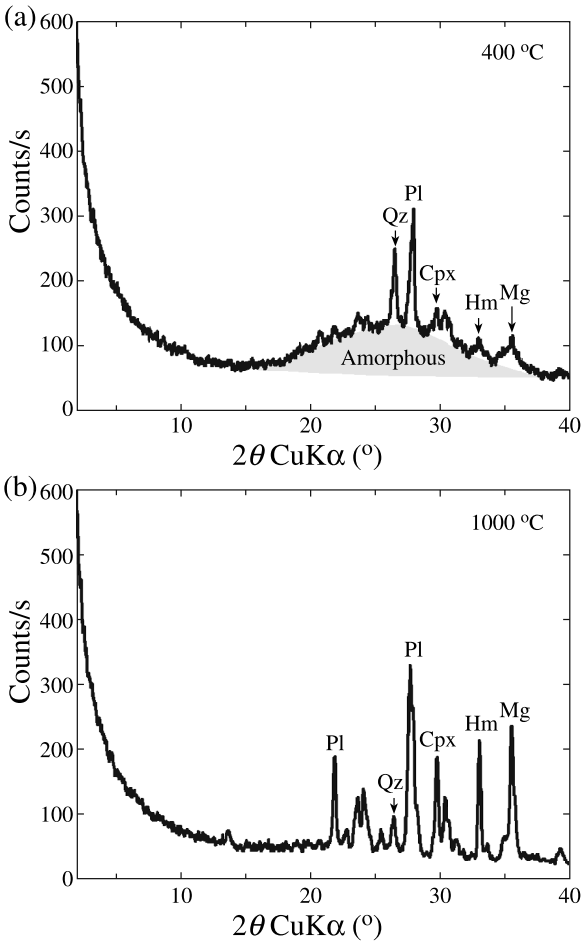

Figure 9. Powder X-ray diffraction charts of the (a) gouge of HTVR014 (400°C) and (b) material on the sliding surface of HTVR015 (1000°C). Pl, plagioclase; Cpx, clinopyroxene; Qz, quartz; Hm, hematite; Mg, magnetite; Amorphous, amorphous material.

power law grain size distribution down to a few tens of nm [e.g., *Chester et al.*, 2005; *Ma et al.*, 2006]. It is therefore difficult to ascribe the observed broad peak to the presence of crystalline particles smaller than a few nm. In contrast, such a broad peak is absent in the material on the sliding surface at T_{meas} of 1000°C (Figure 9b), implying that the material is composed of crystalline particles.

[26] We also have done quantitative analyses following the method described by *Chung* [1974]. We used quartz as the reference mineral, and prepared a powder mixture of equally weighing synthetic quartz and each mineral contained within the material to be analyzed. Amorphous silica was used for the amorphous material. From an X-ray diffraction profile of each mixture, the peak-height ratio of a specific diffraction plane of each mineral to that of quartz was obtained. The peak-height ratio of the same diffraction planes from an X-ray diffraction profile of the material to be analyzed then provides an estimate of relative weight of that specific mineral with respect to quartz. This method, although not so precise, gives a rough estimate of the modal composition in weight percentage.

[27] The results of quantitative analyses are shown in Table 3. The wear materials at T_{meas} below 600°C are largely composed of amorphous phase. With increasing T_{meas}, the content of amorphous phase increases from ≈55 wt% at RT to 76 wt% at 200°C, then decreases from 69 wt% at 400°C to ≈23 wt% at 800°C. The contents of crystalline phases tend to change oppositely. Among the crystalline phases, the relative content of hornblende decreases while those of magnetite and hematite increase. The changes in relative content of other minerals are found to be minor. In the material on the sliding surface at T_{meas} of 1000°C, amorphous phase is absent. In spite of as much as ≈32 vol% pyroxenes in the protolith, the material contains only ≈16 wt% pyroxenes. In contrast, although magnetite and hematite in the protolith are less than 3 vol%, they are over 30 wt% in the material.

3.4. Crystallographic Orientation Analyses

[28] We have measured crystallographic orientations in two small areas in the sample HTVR015 at T_{meas} of 1000°C by using the electron backscatter diffraction (EBSD) technique [e.g., *Randle*, 2003] at Kochi Core Center. One is in a symplectite rim of a clinopyroxene grain in the host rock, while another is in the material on the sliding surface. Both areas are 9.1 μm × 7.3 μm in size, where crystallographic orientation mapping with a step of 0.1 μm has been conducted. Because of poor quality of electron backscatter diffraction images, only orientations of clinopyroxene, magnetite and hematite in the symplectite, and that of hematite in the material on the sliding surface could be determined. Electron backscatter diffraction patterns are manually indexed to determine crystallographic orientations precisely. The results are shown in Figure 10.

[29] In the symplectite, clinopyroxene exhibits mostly a single orientation (Figure 10a), which must be the orientation of the host clinopyroxene grain. Magnetite also shows a single orientation (Figure 10b). Two colors shown in the map (Figure 10b, left) reflect a subtle change in Euler angles, but their orientations are essentially the same (Figure 10b, right). The electron backscatter diffraction pattern of the magnetite looks similar to that of the clinopyroxene, so they likely have an intimate crystallographic relationship. In contrast, hematite grains have different orientations (Figure 10c). They are 0.5 to 2 μm in size. In the material on the sliding surface,

Table 3. Modal Compositions in Weight Percent of the Wear Materials From Room Temperature to 800°C and of the Material on the Sliding Surface at 1000°C[a]

Mineral Species	Room Temperature	200°C	400°C	600°C	800°C	1000°C
Quartz	4.0	3.7	3.4	4.9	5.8	1.5
Feldspars	15.6	10.1	9.2	18.9	27.1	50.3
Biotite	0.1	0.0	0.4	0.5	0.3	0.0
Hornblende	6.4	2.7	2.0	3.4	2.9	0.0
Pyroxenes	11.0	3.1	6.7	12.2	19.4	15.9
Magnetite	5.0	2.9	4.6	8.6	13.7	15.8
Hematite	2.0	0.0	3.2	4.2	8.3	15.6
Ilmenite	1.3	1.6	1.5	0.0	0.0	0.9
Amorphous	54.7	76.0	69.0	47.3	22.6	0.0
Total	100.1	100.1	100.0	100.0	100.1	100.0

[a]Feldspars include plagioclase and K-feldspar, while pyroxenes include clinopyroxene and orthopyroxene.

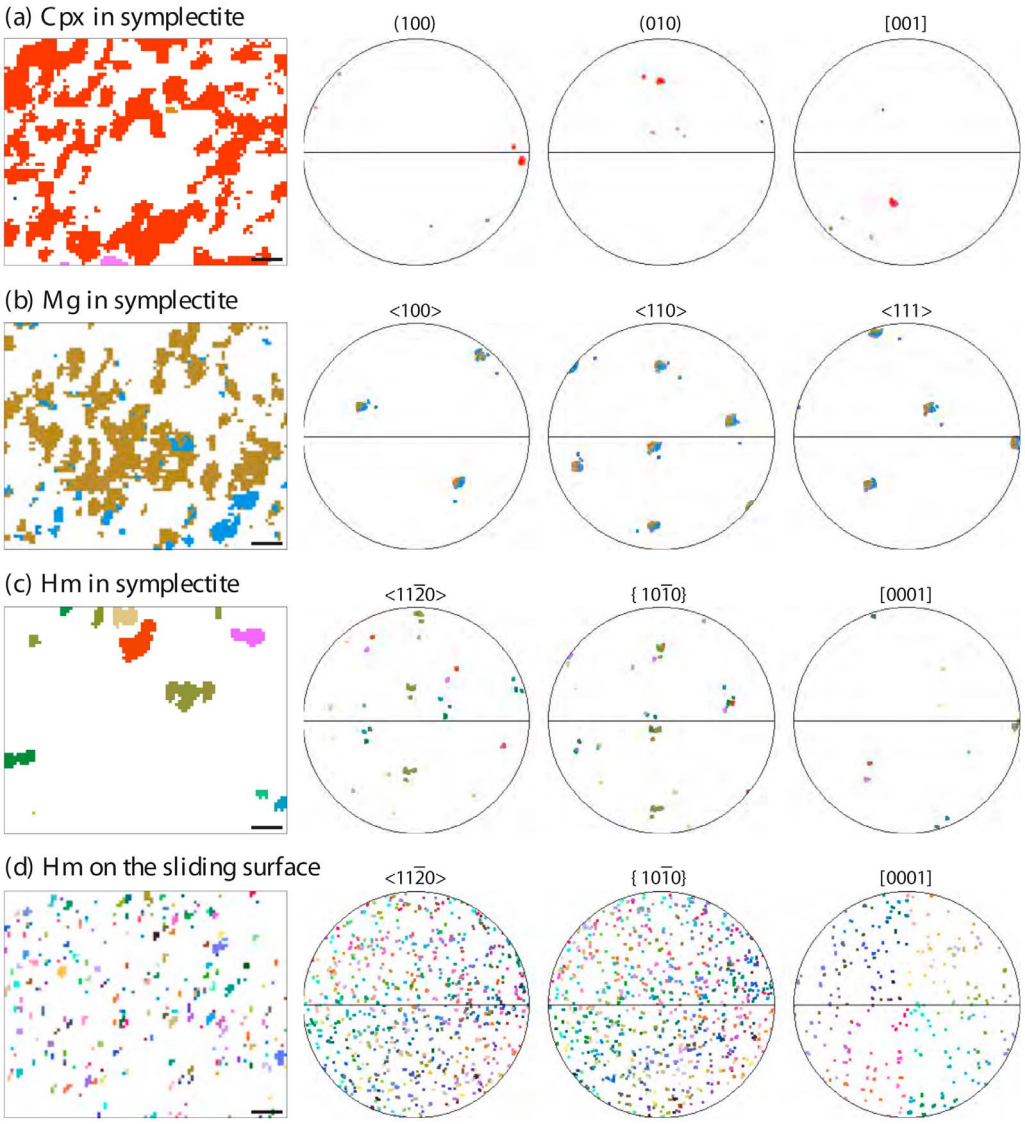

Figure 10. (left) Crystallographic orientation map and (right) equal area, lower hemisphere projections of three crystallographic directions indicated, obtained from the sample of HTVR015 (1000°C). (a) Clinopyroxene, (b) magnetite, and (c) hematite from an area of symplectite in the host rock. (d) Hematite from an area in the material on the sliding surface. Scale bars in crystallographic orientation maps are 1 μm in length. In each equal area projection, horizontal line and its ends represent the orientations of the sliding surface and the slip direction, respectively.

hematite grains are as small as 0.1 μm in size and scattered (Figure 10d, left). Their orientations are almost random (Figure 10d, right).

4. Comparison of HTVR and HVR

[30] In HTVR runs, there is no remarkable slip weakening (Figure 2) which is typically observed in high-velocity friction experiments at fixed slip rates [e.g., *Hirose and Shimamoto*, 2005; *Mizoguchi et al.*, 2007; *Sone and Shimamoto*, 2009] and also in the HVR runs at relatively high V (Figure 4a). In HTVR runs, the change in the macroscopic temperature due to frictional heating on the simulated fault is much smaller than HVR runs because of the control in temperature near the simulated fault and the low frictional heat generation. HTVR runs have demonstrated that f at the steady state depends on T at constant V. Then the slip weakening observed in HVR runs (e.g., Figure 4a) as well as in previous studies are likely caused by frictional heating and increase in T during experiments. *Mizoguchi et al.* [2007] showed that the experimentally observed slip-weakening distance decreases with increasing normal stress for clay-bearing natural fault gouges, implying that a rapid temperature rise causes rapid weakening of a fault. It should be noted that the weakening mechanism is probably different for different rocks. Further studies are therefore needed to show if the increase in T is always responsible for the slip weakening observed in the previous experimental studies.

[31] *Tsutsumi and Shimamoto* [1997a] conducted a series of frictional experiments at high slip rates and revealed the

strong "rate-weakening" behavior in the steady state under conditions without generation of a melt layer. In their experiments, f decreases from around 0.8 to around 0.5 with increasing V from 0.01 m/s to 0.55 m/s (Figure 5b), and a further increase in V higher than 0.73 m/s causes the onset of melting associated with strengthening due to generation of melt patches [*Hirose and Shimamoto*, 2005]. Note that T is not controlled in their experiments and probably substantially high at 0.55 mm/s in the steady state. The HVR runs conducted in this study shows similar "rate-weakening" behavior associated with the increase in T (Figure 5a).

[32] Figure 5a shows the comparison of the experimental results using HTVR and HVR projected onto a (T, f) plane. For readability, only HTVR016 is plotted among the HTVR runs. It should be noted that the friction coefficient at low temperature is generally higher in HVR than HTVR by about 0.1. This is possibly due to the strength of an O ring which seals the sample chamber of HTVR.

[33] Except the data at V = 0.414 m/s with HVR, the weakening rate with increasing temperature, the slope in Figure 5a, is similar between HTVR and HVR runs although V ranges for more than one order of magnitude for HVR runs while the V is kept at 0.010 m/s for HTVR runs. This indicates that the effect of temperature is probably more important than that of V in this regime. In Figure 5b, the range of f for HTVR is comparable to that for HVR at V smaller than 0.3 m/s. The data at V = 0.414 m/s shows significantly lower value of f than HTVR runs and the extrapolation of the other HVR runs (Figure 5b). Therefore, it is likely that the effect of V becomes significant between V = 0.3 m/s and 0.4 m/s.

[34] Given that f depends not only on V, but also on T, then the steady state friction coefficient as well as the transient behavior (e.g., slip-weakening distance) in those experiments depends on the thermal properties of the surrounding system, or an apparatus because they affect the temperature distribution at the steady state. Considering application to numerical studies for earthquake rupture propagation which takes place at much higher normal stress than experimental conditions and has complicated slip rate history, it is important to extract the properties of a simulated fault separately from effects of different apparatus. The control or at least monitoring T is critically important for such a purpose.

5. Discussion

[35] Figure 11 shows f for the HTVR runs as well as the contents of amorphous phase and magnetite plus hematite plotted as a function of T_{meas}. It is apparent that f below 800°C has a negative correlation with the amount of amorphous phase. The decrease in f from RT to 400°C corresponds to the increase in the amount of amorphous phase, while the increase in f from 400°C to 800°C corresponds to the decrease in amount of amorphous phase. Hence the generation of amorphous phase is likely to cause the weakening. At a temperature range between 200°C and 400°C, wear materials contain amorphous phase as large as 70 wt% (Table 2 and Figure 11), so f is likely to be controlled by the weak amorphous phase. However, although amorphous phase at RT (≈55 wt%) is similar in amount to that at 600°C (≈47%), f at RT (between 0.7 and 0.8) is much higher than f at 600°C (≈0.6), which cannot be explained solely by the amount of amorphous phase.

[36] A series of experiments with various T_{meas} HTVR017 provides further insights. Once the sample was heated from 50°C to 500°C, the reduced f did not recover when cooled down to 50°C again. Note that between runs at different temperatures, the sliding surface is not opened and no presliding has been performed. Therefore, the sliding surfaces developed at RT and at 500°C have different mechanical properties, and the former is overwritten by the latter but the latter isn't by the former in the experimental time scale. One possibility is irreversible generation of weak material at high temperature, such as larger amount of amorphous material and more oxidized material than at RT. Another possibility is moisture-drained weakening [*Mizoguchi et al.*, 2006]; when the sample is heated up to 500°C, moisture would be lost from the sliding surface, and therefore f is reduced by loosing moisture from the sliding surface. Absorbing moisture onto the sliding surface when the sample is cooled down may take a certain amount of time, so f may not recover during sliding after cooling down to 50°C. In other words, f at RT and 50°C is high due to the moisture-absorbing strengthening [*Mizoguchi et al.*, 2006]. In order to determine the weakening mechanisms relevant from RT to higher temperature, further investigation is needed.

[37] *Noda* [2008] derived a friction constitutive law based on a microscopic slip process at asperities which requires thermal activation [*Nakatani*, 2001; *Rice et al.*, 2001] with neglecting contact growth. This law predicts linear decrease in f with increasing T, which is sometimes observed for ceramics [*Senda*, 2004]. In the present study, however, the temperature weakening is observed only from RT to 400°C and above 800°C, while f increases with T_{meas} between these regimes. Also, the model by *Noda* [2008] has no memory effect for a history of T, and neglects the nonreversible processes such as reactions at high T, failing to explain a series of experiments with cycles in T_{meas} (HTVR017).

[38] The decrease in amount of amorphous phase and hence the increase in f from 400°C to 800°C likely correspond to the increase in amount of magnetite and hematite in wear materials, which can be ascribed to progressive oxidation of wear materials as well as of samples. Progressive oxidation with increasing T is apparent from the change in color of wear materials (Figure 6) and as well as that of hornblende (Figure 7). Increasing amount of magnetite and hematite with decreasing amount of amorphous phase implies that comminution of magnetite and hematite does not produce amorphous phase.

[39] Because amorphous phase is absent in the material on the sliding surface at 1000°C, the decrease in f above 800°C cannot be explained by the amount of amorphous phase, either. The symplectite rims of clinopyroxene grains (Figures 8e and 8f) indicate that decomposition of clinopyroxene into magnetite, hematite, plagioclase and relict clinopyroxene occurred at 1000°C. The material on the sliding surface contains these minerals and quartz (Figures 8d and 8b), and therefore it is likely to be derived from symplectitic aggregates. Constituent grains in the material are mostly smaller than 1 μm in size, rounded and equant, and rather homogeneously mixed (Figure 8d). Hematite grains are dispersed and randomly oriented (Figure 10d). These together with the flowage and folded structure (Figure 8c)

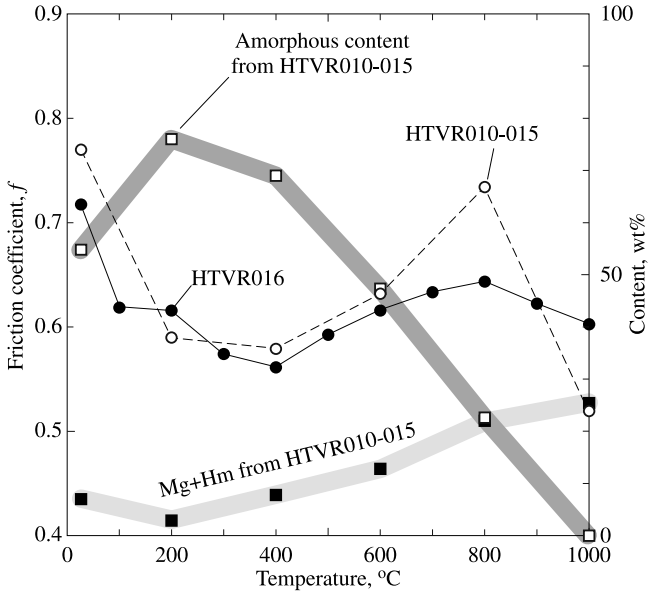

Figure 11. Friction coefficient and contents of amorphous phase, magnetite and hematite plotted as a function of temperature. Open and filled circles denote the friction coefficients for HTVR010–015 and HTVR016, while open and filled squares denote the contents of amorphous phase and magnetite plus hematite, respectively.

suggest granular flow on the sliding surface. Decomposition reaction of clinopyroxene requires grain boundary diffusion, which likely has accommodated grain boundary sliding leading to granular flow of reaction products. The reduced f above 800°C may thus be ascribed to granular flow of reaction products derived from decomposition of clinopyroxene.

6. Conclusions

[40] A rotary shear apparatus with a temperature control has been set up at Chiba University. Frictional experiments and microscopic observations for dolerite at a normal stress, σ_n = 1 MPa, a fixed slip rate, V = 0.010 m/s, and different temperature, T_{meas}, ranging from room temperature (RT) to 1000°C, have revealed the followings. With increasing T_{meas}, the friction coefficient, f, decreases from around 0.7–0.8 at RT to 0.5–0.6 at T_{meas} = 400°C, increases until T_{meas} = 800°C, and then decrease again. X-ray diffraction analyses of wear materials revealed the presence of amorphous phase as large as 76 wt%, and the amount of amorphous phase in the wear materials has a negative correlation to f except at RT and above 800°C. The generation of amorphous phase causes the weakening, and an increase in amount of amorphous phase results in a decrease in f. The decrease in amount of amorphous phase above 400°C and hence the increase in f correspond to the increase in amount of magnetite and hematite due to progressive oxidation, comminution of which does not likely produce amorphous phase. One possible mechanism for high f at RT is moisture strengthening although further experimental investigation is needed. The decrease in f above 800°C is likely due to granular flow of reaction products derived from decomposition of clinopyroxene. Comparison of the mechanical data with a series of experiments at various V and without active control on, but with measurement of the temperature have revealed that the apparent rate weakening at V < 0.3 m/s can be explained by the temperature effect. The experiments presented in this study have illuminated a significant effect of temperature on the fault on the friction coefficient separately from that of slip rate. This effect probably has a rather large contribution to the strong "rate weakening" which was often observed in many frictional experiments at coseismically high slip rates.

[41] **Acknowledgments.** We are sincerely grateful to T. Senda for his efforts to develop the apparatus and to move it to Chiba University, T. Shimamoto for his suggestions and efforts in arranging the setup of the apparatus, and T. Umino for her assistance with observations and analyses of samples and wear materials. We appreciate the comments by reviewers (N. De Paola and an anonymous reviewer) and by the Associate Editor D. Faulkner which improved this paper. This work is partly supported by Earthquake Research Institute, the University of Tokyo, through funds 2007-A-13 and 2008-A-14 in moving the apparatus from National Maritime Institute of Japan to Chiba University. This work is also supported by MEXT grant #21107004 and JSPS grant #23340151.

References

Beeler, N. M., T. E. Tullis, and D. L. Goldsby (2008), Constitutive relationships and physical basis of fault strength due to flash heating, *J. Geophys. Res.*, *113*, B01401, doi:10.1029/2007JB004988.

Blanpied, M. L., D. A. Lockner, and J. D. Byerlee (1995), Frictional slip of granite at hydrothermal conditions, *J. Geophys. Res.*, *100*, 13,045–13,064, doi:10.1029/95JB00862.

Byerlee, J. D. (1978), Friction of rocks, *Pure Appl. Geophys.*, *116*, 615–626, doi:10.1007/BF00876528.

Chester, F. M. (1994), Effects of temperature on friction: Constitutive equations and experiments with quartz gouge, *J. Geophys. Res.*, *99*, 7247–7261, doi:10.1029/93JB03110.

Chester, J. S., F. M. Chester, and A. K. Kronenberg (2005), Fracture surface energy of the Punchbowl fault, San Andreas system, *Nature*, *437*, 133–136, doi:10.1038/nature03942.

Chung, F. H. (1974), Quantitative interpretation of X-ray diffraction patterns. I. Matrix-flushing method of quantitative multicomponent analysis, *J. Appl. Cryst.*, *7*, 519–525, doi:10.1107/S0021889874010375.

Fukuchi, T., K. Mizoguchi, and T. Shimamoto (2005), Ferrimagnetic resonance signal produced by frictional heating: A new indicator of paleoseismicity, *J. Geophys. Res.*, *110*, B12404, doi:10.1029/2004JB003485.

Goldsby, D. L., and T. E. Tullis (2002), Low frictional strength of quartz rocks at subseismic slip rates, *Geophys. Res. Lett.*, *29*(17), 1844, doi:10.1029/2002GL015240.

Hamada, Y., T. Hirono, M. Ikehara, W. Soh, and S.-R. Song (2009), Estimated dynamic shear stress and frictional heat during the 1999 Taiwan Chi-Chi earthquake: A chemical kinetics approach with isothermal heating experiments, *Tectonophysics*, *469*, 73–84, doi:10.1016/j.tecto.2009.01.036.

Han, R., T. Shimamoto, T. Hirose, J. H. Ree, and J. Ando (2007), Ultralow friction of carbonate faults caused by thermal decomposition during seismic slip, *Science*, *316*, 878–881, doi:10.1126/science.1139763.

Hirose, T., and T. Shimamoto (2005), Growth of molten zone as a mechanism of slip weakening of simulated faults in gabbro during frictional melting, *J. Geophys. Res.*, *110*, B05202, doi:10.1029/2004JB003207.

Kano, Y., J. Mori, R. Fujio, H. Ito, T. Yanagidani, S. Nakao, and K. F. Ma (2006), Heat signature on the Chelungpu fault associated with the 1999 Chi-Chi, Taiwan earthquake, *Geophys. Res. Lett.*, *33*, L14306, doi:10.1029/2006GL026733.

Ma, K.-F., et al. (2006), Slip zone and energetics of a large earthquake from the Taiwan Chelungpu-fault drilling project, *Nature*, *444*, 473–476, doi:10.1038/nature05253.

Mizoguchi, K., T. Hirose, T. Shimamoto, and E. Fukuyama (2006), Moisture-related weakening and strengthening of a fault activated at seismic slip rates, *Geophys. Res. Lett.*, *33*, L16319, doi:10.1029/2006GL026980.

Mizoguchi, K., T. Hirose, T. Shimamoto, and E. Fukuyama (2007), Reconstruction of seismic faulting by high-velocity friction experiments: An example of the 1995 Kobe earthquake, *Geophys. Res. Lett.*, *34*, L01308, doi:10.1029/2006GL027931.

Murakami, M., and T. Tagami (2004), Dating pseudotachylyte of the Nojima fault using the zircon fission-track method, *Geophys. Res. Lett.*, *31*, L12604, doi:10.1029/2004GL020211.

Nakatani, M. (2001), Conceptual and physical clarification of rate- and state-dependent friction law: Frictional sliding as a thermally activated rheology, *J. Geophys. Res.*, *106*, 13,347–13,380, doi:10.1029/2000JB900453.

Noda, H. (2008), Frictional constitutive law at intermediate slip rates accounting for flash heating and thermally activated slip process, *J. Geophys. Res.*, *113*, B09302, doi:10.1029/2007JB005406.

Noda, H., and N. Lapusta (2010), Three-dimensional earthquake sequence simulations with evolving temperature and pore pressure due to shear heating: Effect of heterogeneous hydraulic diffusivity, *J. Geophys. Res.*, *115*, B12314, doi:10.1029/2010JB007780.

Noda, H., E. M. Dunham, and J. R. Rice (2009), Earthquake ruptures with thermal weakening and the operation of major faults at low overall stress levels, *J. Geophys. Res.*, *114*, B07302, doi:10.1029/2008JB006143.

O'Hara, K. (2004), Paleo-stress estimates on ancient seismogenic faults based on frictional heating of coal, *Geophys. Res. Lett.*, *31*, L03601, doi:10.1029/2003GL018890.

Prakash, V., and R. J. Clifton (1992), Pressure-shear plate impact measurement of dynamic friction for high speed machining applications, paper presented at Seventh International Congress on Experimental Mechanics, Soc. of Exper. Mech., Bethel, Conn.

Randle, V. (2003), *Microtexture Determination and Its Applications*, 2nd ed., 138 pp., Maney, London.

Rice, J. R. (1999), Flash heating at asperity contacts and rate-dependent friction, *Eos Trans. AGU*, *80*(46), Fall Meet., Suppl., F681l.

Rice, J. R. (2006), Heating and weakening of faults during earthquake slip, *J. Geophys. Res.*, *111*, B05311, doi:10.1029/2005JB004006.

Rice, J. R., N. Lapusta, and K. Ranjith (2001), Rate and state dependent friction and the stability of sliding between elastically deformable solids, *J. Mech. Phys. Solids*, *49*, 1865–1898, doi:10.1016/S0022-5096(01)00042-4.

Senda, T. (2004), Study on sliding friction and wear of ceramics at elevated temperatures (in Japanese with English abstract), Ph.D. thesis, 190 pp., Tokyo Inst. of Technol., Tokyo.

Senda, T., J. Drennan, and R. McPherson (1992), Wear and friction of alumina at elevated temperatures, in *Ceramics Adding the Value, Proceedings of the International Ceramics Conference*, edited by B. J. Bannister, pp. 932–937, Commonw. Sci. and Ind. Res. Org., East Melbourne, Australia.

Senda, T., J. Drennan, and R. McPherson (1995), Sliding wear of oxide ceramics at elevated temperatures, *J. Am. Ceram. Soc.*, *78*(11), 3018–3024, doi:10.1111/j.1151-2916.1995.tb09077.x.

Shimamoto, T. (1986), Strengthening of phyllosilicate and gypsum gouges with increasing temperature: Effect of temperature or moisture elimination?, *Int. J. Rock. Min. Sci. Geomech. Abstr.*, *23*(6), 439–443, doi:10.1016/0148-9062(86)92309-0.

Sone, H., and T. Shimamoto (2009), Frictional resistance of faults during accelerating and decelerating earthquake slip, *Nat. Geosci.*, *2*, 705–708, doi:10.1038/ngeo637.

Tanaka, H., W. M. Chen, C. Y. Wang, K. F. Ma, N. Urata, J. Mori, and M. Ando (2006), Frictional heat from faulting of the 1999 Chi-Chi, Taiwan earthquake, *Geophys. Res. Lett.*, *33*, L16316, doi:10.1029/2006GL026673.

Tsutsumi, A., and T. Shimamoto (1997a), High velocity frictional properties of gabbro, *Geophys. Res. Lett.*, *24*, 699–702, doi:10.1029/97GL00503.

Tsutsumi, A., and T. Shimamoto (1997b), Temperature measurement along simulated faults during seismic fault motion, *Proc. Int. Geol. Congr.*, *30th*, 223–232.

Yund, R. A., M. L. Blanpied, T. E. Tullis, and J. D. Weeks (1990), Amorphous material in high strain experimental fault gouges, *J. Geophys. Res.*, *95*, 15,589–15,602, doi:10.1029/JB095iB10p15589.

T. Hirose, Kochi Institute for Core Sample Research, Japan Agency for Marine-Earth Science and Technology, Nangoku 783-8502, Japan.

A. Inoue and K. Kanagawa, Department of Earth Sciences, Chiba University, Chiba 263-8522, Japan.

H. Noda, Institute for Research on Earth Evolution, Japan Agency for Marine-Earth Sciences and Technology, 3173-25 Showa-machi, Kanazawa-ku, Yokohama 236-0001, Japan. (hnoda@jamstec.go.jp)